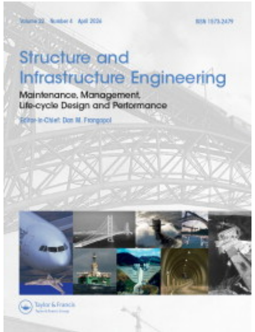

Taylor & Francis
Taylor & Francis Group

Structure and Infrastructure Engineering
Maintenance, Management, Life-Cycle Design and Performance

ISSN: 1573-2479 (Print) 1744-8980 (Online) Journal homepage: www.tandfonline.com/journals/nsie20

Proposal of an effective modelling strategy for the advanced numerical analysis of masonry arch-bridges

Giuseppina Uva , Luigi S. Rainone , Luis C.M. da Silva & Siro Casolo

To cite this article: Giuseppina Uva , Luigi S. Rainone , Luis C.M. da Silva & Siro Casolo (26 May 2026): Proposal of an effective modelling strategy for the advanced numerical analysis of masonry arch-bridges, Structure and Infrastructure Engineering, DOI: 10.1080/15732479.2026.2672966

To link to this article: https://doi.org/10.1080/15732479.2026.2672966

Published online: 26 May 2026.

STRUCTURE AND INFRASTRUCTURE ENGINEERING
https://doi.org/10.1080/15732479.2026.2672966

Proposal of an effective modelling strategy for the advanced numerical analysis of masonry arch-bridges

Giuseppina Uva[a], Luigi S. Rainone[a], Luis C.M. da Silva[b] and Siro Casolo[b]

[a]DICATECh Department, Politecnico di Bari, Bari, Italy; [b]ABC Department, Politecnico di Milano, Milano, Italy

ABSTRACT

This study investigates the numerical analysis of masonry arch bridges, a process often challenged by various sources of uncertainty that can compromise the reliability of results. A streamlined approach is proposed through the calibration of a simplified finite element model. The San Marcello Pistoiese bridge (Italy) serves as a case study, benefiting from extensive prior documentation, including laboratory testing and dynamic identification, which enables the validation of numerical simulations against experimental data. Two models were developed: a detailed three-dimensional solid model and a simplified shell model. Both employ the Concrete Damage Plasticity (CDP) approach to capture non-linear behaviour, using a bilinear stress-strain relationship up to peak strength, followed by a post-peak softening response in accordance with the Model Code. The shell model was calibrated against the solid model based on modal characteristics and subsequently used for non-linear analyses. Results show that the reduced model effectively reproduces key aspects of the structural response - such as capacity curves and damage patterns - while requiring only 1/500 of the computational time, making it a practical tool for extensive parametric studies under uncertainty.

ARTICLE HISTORY
Received 15 July 2025
Revised 17 January 2026
Accepted 26 February 2026

KEYWORDS
Masonry arch bridges; finite elements; non-linear modelling; concrete damage plasticity; modelling strategies; reduced calibrated models; uncertainty

1. Introduction

The structural analysis of historical masonry arch-bridges (Figure 1) is typically conditioned by multiple sources of uncertainty that can affect the reliability of the results, including the incomplete knowledge of the original design and construction processes (often dating back to ancient times), the layering of interventions and structural modifications over time, the presence of structural elements and material parts that are partially hidden and difficult to access, the presence of infill granular material with a very variable nature and composition, the progression of damage and degradation process over time.

In order to define an accurate structural model, the actual geometric features, constructive details, material properties and mechanical parameters should be characterised on site by resorting to specific surveys and diagnostic techniques, both destructive and non-destructive. Such activities, however, may be time consuming, expensive and possibly invasive, can never be completely exhaustive, especially in the case of historical masonry structures, that are typically inhomogeneous and characterised by diversified phenomena of degradation and erosion. Systematic destructive tests and surveys are not acceptable, because of safety and conservation issues, and this means that the knowledge frame is inevitably uncomplete. Moreover, it is worth remembering that masonry is characterised by a strongly non-linear response, progressive damage and degradation of stiffness and strength and that the spatial uncertainty in the identification of constitutive parameters in the non-linear field is even higher, also considering the lack of reliable specific experimental procedures. A further source of uncertainty regards the definition of the static and seismic loads, that would require a proper approach to account for the record variability.

There is a wide scientific literature about the abovementioned uncertainties issues, regarding the definition of the geometrical and material models for masonry structures (Casolo & Sanjust, 2009; Crisafulli et al., 2005; D'Altri et al., 2020; Giaretton et al., 2016; Oliveira et al., 2010; Zizi et al., 2023), the characterisation of the mechanical properties of materials accounting for degradation due to atmospheric phenomena and damage (Modena et al., 2015; Tubaldi et al., 2020), the modelling of actions - including erosive phenomena, soil-structure interaction; the variability in space and time of seismic action (Bayraktar & Hökelekli, 2021; Casolo et al., 2017; Gönen & Soyöz, 2021; Smith et al., 2004; Zani et al., 2020).

An appropriate modelling strategy should be able to adequately represent all the above-mentioned aspects, but this usually involves the development and management of complex numerical models and time-consuming calculation processes. Several modelling strategies (Caliò et al., 2012; Drygala et al., 2018; Liu et al., 2023; Rinaldin et al., 2016) and computing software exist, capable of simulating structural behaviour in both static and dynamic conditions, taking into account complex phenomena such as contact

CONTACT Giuseppina Uva Giuseppina.uva@poliba.it DICATECh Department, Politecnico di Bari, Bari, Italy.

Figure 1. Typical defects and critical issues that can be found in real case studies (from top, left to bottom, right): environment agents-induced degradation and material voids; impact damages and erosion; longitudinal cracks.

between structural elements (Forgács et al., 2018) or damage evolution (Addessi et al., 2021; 2022; Casolo & Peña, 2007; Tecchio et al., 2023). Such methods, however, are very demanding in terms of implementation effort and computation time, and are therefore unpractical, especially if they are to be used in a professional context.

It is evident, therefore, that the effort to achieve greater accuracy and reliability by implementing models of great complexity and detail may be hampered by the presence of input data characterised by such high uncertainties. A realistic strategy to account for epistemic uncertainty related to model data would require a sensitivity analysis on the parameters involved, both mechanical and geometric, generating a large number of structural models varying these parameters and appraising the effect in terms of capacity. The number of numerical analyses involved becomes very large, and typically, it is not feasible to perform them within a reasonable time frame if complex models are used.

The approach presented in this paper stems from these observations and aims to reduce the complexity and burden of analyses by developing simplified 3D models appropriately calibrated to capture the relevant features of the structural behaviour of the bridge under seismic actions and that can be used in the extensive analyses of masonry arch bridges and assess uncertainty both in the modelling aspect and in the seismic loads. With this objective, a modelling strategy is proposed and applied on the real case-study of San Marcello Pistoiese bridge (Pistoia, Italy). For this bridge, detailed geometrical data are available, together with the results of experimental laboratory and field tests that were performed to characterise mechanical parameters and dynamic properties of the structure (Leprotti et al., 2010; Pelà et al., 2009; 2013). In particular, a non-destructive dynamic identification procedure was carried out to provide the experimental reference values of the dynamic structural properties and validate numerical models.

In the numerical modelling procedure proposed, two types of Finite Element (FE) models were developed in Abaqus environment (Dassault Systemes Simulia Corporation, 2011), and modal and non-linear pushover analyses were performed. The first model, which will be referred to as "Solid Model", is a complete three-dimensional solid FE model, with all structural elements realistically described with their actual geometry. This model was validated by exploiting field test data about materials and results of experimental dynamic identification. The second model, referred to as "Shell-Box Model", is also a three-dimensional FE model but features a simplified geometry reproduced by fictitious shell elements, so to reduce the number of degrees of freedom of the problem and perform a great number of parametric analyses. The calibration of the reduced order model with regard to geometry, masses, mechanical parameters (in the elastic and inelastic field) of the shell elements has been made by using as a reference the Solid Model. In both cases, for modelling the non-linear damage response, the Concrete Damage Plasticity model (Lee & Fenves, 1998; Lubliner et al., 1989) has been implemented, which is an advanced approach able to simulate the development of damage in masonry-like structures as the loading history evolves.

The capability of the simplified model to reproduce the "accurate" results of the complete one has been tested by systematically comparing the results of the analyses with regard to five aspects: (1) inertial characteristics; (2) modal parameters (periods, shape of vibration modes); (3) design spectral acceleration according to the spectra of the Italian Building Code (Ministero delle Infrastrutture e dei Trasporti, 2018, 2019); (4) capacity curves; (5) damage maps. The case study selected to illustrate the modelling strategy is particularly significant, as it represents a recurring bridge typology in Italy and for which, moreover, are available not only experimental results on materials - obtained through laboratory and field tests, but also data from a dynamic identification test. The latter allowed for the characterisation of the dynamic response of the structure under the application of an impulsive force, enabling the identification of the main modal parameters, which are a fundamental reference for validating numerical models. As widely recognised when modelling and assessing existing structures - especially masonry ones - such information is not sufficient to significantly reduce the uncertainty associated with the materials and their mechanical parameters, that remains high due to the intrinsic scattering of experimental data and their spatial heterogeneity within the structure, particularly in areas that cannot be directly inspected.

Dynamic identification tests represent an essential complementary tool as they enable a more accurate calibration of elastic parameters, despite some limitations. In the case at hand, the outcomes of identification are limited to the elastic domain, since the impulsive force was generated by a vehicle passing over an artificial bump and abruptly changing direction - a scenario incapable of activating the post-elastic response and characterise the associated non-linear parameters. Thus, in the absence of direct experimental tests useful for the non-linear range, the related parameters can only rely on existing literature and engineering judgement, and it becomes essential to conduct extensive parametric analyses to assess the effects of uncertain input parameter on the structural response. The proposed strategy is particularly well-suited for this purpose, as it enables the development of fairly accurate and computationally efficient numerical models to support large-scale parametric studies, facilitating the derivation of fragility curve families and effectively integrating the available experimental data for practical, real-world applications.

2. Presentation of the case study: the masonry arch bridge of San Marcello Pistoiese, Italy

The case study considered for the demonstration of the modelling approach is the San Marcello Pistoiese bridge, located in the homonymous municipality in the province of Pistoia (Tuscany, Italy), whose typological features and masonry materials are very recurrent in the Italian context. The geometrical and mechanical data presented in this section are taken from literature (Leprotti et al., 2010; Pelà et al., 2009; 2013). The reader is addressed to the mentioned works for further information. The bridge was built after the Second World War to cross the Lima River using various types of masonry materials and arrangements (Table 1) and is characterised by the presence of an infill consisting of waste material obtained from the excavation of the foundations.

The main structure is composed of three arches. The central arch is the largest one and has a radius of 10.75 m. The springing line of the central arch is located at a height of 10 m from the ground line (i.e., from the upper surface of the shallow foundations of the central piles). The axis of this arch constitutes a straight symmetry axis for the whole structure. The two side arches have a radius of 4.00 m and have a variable height between 7.00 and 17.00 m in relation to the morphology of the ground. The piles and abutments rest on reinforced concrete elements. The foundations are shallow and rest on a stable rocky ground. The structure has a maximum height of 24.25 m and an overall longitudinal development of 72.50 m, with a thickness of 5.80 m (Figure 2 top). A peculiar element of the structure is the presence of an infill material between the two external masonry walls having a variable thickness, larger near the arches and smaller near the road level (Figure 2 bottom). The upper surface is bounded by masonry beams.

The available data, including information provided by surveys and experimental investigation, were sufficient for the reconstruction of a satisfactory model geometry, which was implemented by assuming the following assignment of structural materials:

- Piers, spandrel walls, abutments, parapets: stone and lime mortar masonry (“*Masonry 1*”).
- Arch spandrel: stone and concrete mortar masonry (“*Masonry 2*”).
- Vaults: bricks and concrete mortar masonry (“*Masonry 3*”).
- Infill above vaults and between spandrel walls: waste soil-like material obtained from excavation of foundations (“*Infill*”).

Compressive and tensile strength, Young’s modulus, Poisson’ ratio, internal friction angle and cohesion were measured by laboratory and field tests (Pelà et al., 2009) and are summarised in Table 1. Regarding these parameters, the case study presented confirms that the experimental characterisation of materials is a critical point for existing masonry structures: despite the great deal of laboratory and on-site activities carried out, the outcome was that a considerable scattering affected test results, suggesting that parametric analyses on mechanical data are necessary. It should be also mentioned that not all structural materials could be directly investigated, which is very typical of ancient masonry structures, and therefore, in some cases, engineering judgement and reference literature values had to be used (Pelà et al., 2009). The information available from experimental dynamic identification has been used as a reference for the definition of material elastic parameters and restraint conditions in the numerical models developed.

Regarding the modelling of the seismic action, the design acceleration spectra to be used for the case study have been determined according to the Italian Building Code for the Limit State of Life Safety, assuming a Design Life of 50 years and a Use Class III (Figure 3). According to the available literature, the soil type is “A” and the topographic category is “T1”.

3. Strategy for the calibration of effective simplified numerical models

3.1. Constitutive modelling of the elastic response

Regarding the constitutive behaviour in the elastic field, all the materials of the numerical models of the bridge are considered as homogeneous, isotropic continuum, with the parameters listed in Table 2.

3.2. Constitutive modelling of the post-elastic response

The post-elastic response is modelled by using the Concrete Damage Plasticity (hereafter CDP) Model, a material model

Table 1. Mechanical parameters for the four materials of the bridge (Pelà et al., 2009).

Material	Friction angle Φ [°]	Cohesion C [MPa]	Uniaxial tensile strength $\sigma_{t,y}$ [MPa]	Uniaxial compressive strength $\sigma_{c,y}$ [MPa]
Infill	20	0.05	0.070	0.143
Masonry 1	61	0.58	0.299	4.485
Masonry 2	61	0.58	0.299	4.485
Masonry 3	55	0.35	0.221	2.220

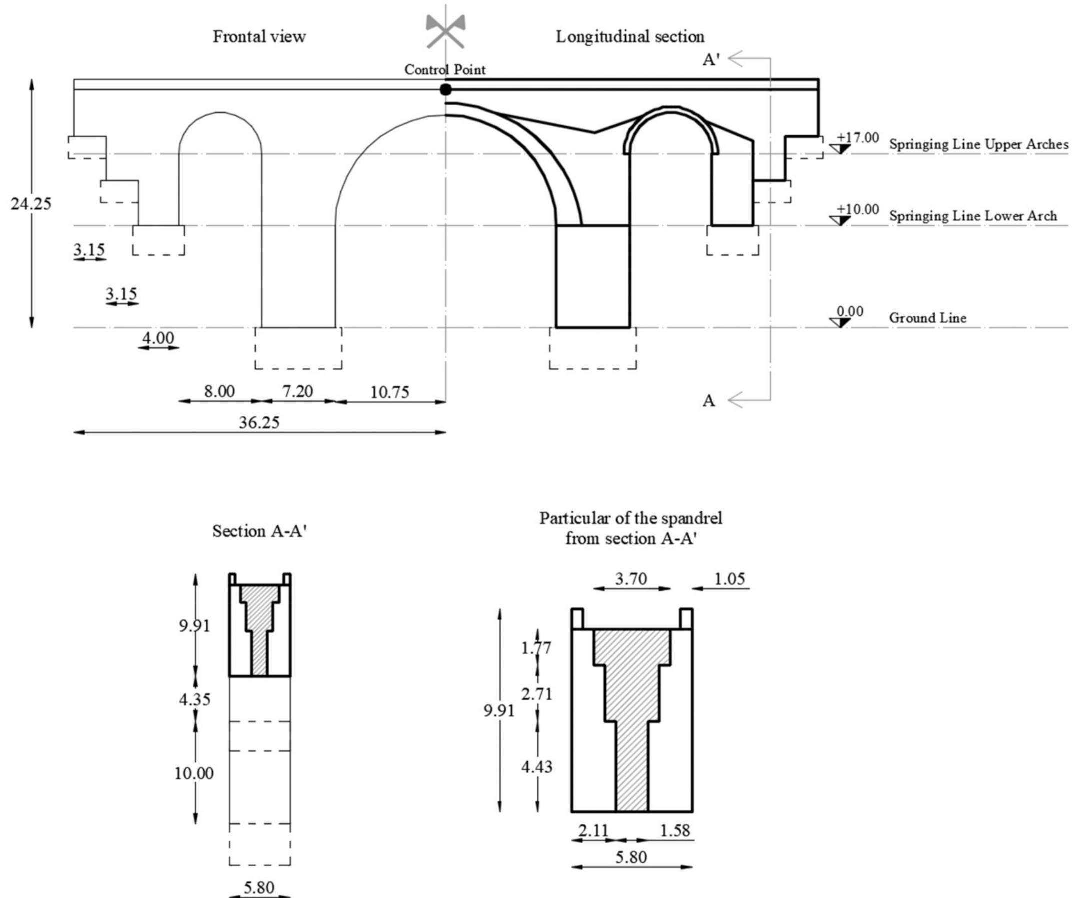

Figure 2. Longitudinal (top) and transversal (bottom) view of the bridge (measures are given in meters).

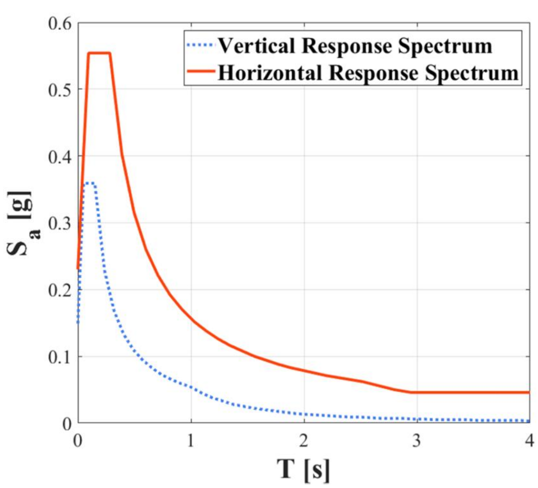

Figure 3. Design spectra at the LS Limit State for the horizontal and vertical components.

Table 2. Densities and elastic modules adopted for materials.

Material	γ [kg/m^3]	E_1 [MPa]	υ [-]	G [MPa]
Infill	1800	1000	0.2	416.67
Masonry 1	2200	10000	0.2	4166.67
Masonry 2	2200	12000	0.2	5000.00
Masonry 3	1800	10000	0.2	4166.67

widely used in recent literature for modelling the behaviour of masonry structures (Casolo et al., 2017; Lee & Fenves, 1998; Lubliner et al., 1989; Rainone et al., 2023). It is a continuum model with damage available in the Abaqus material Library (Dassault Systemes Simulia Corporation, 2011), that allows to model at the macro-scale the effects of the cracking process in concrete-like materials, albeit with appropriate simplifications. It has gained wide popularity because of its ease of handling without requiring the use of complex tools such as user-defined subroutines. In this study, the materials indicated as "*Masonry 1*", "*Masonry 2*" and "*Masonry 3*" have been modelled using CDP both for compressive and tensile behaviour. For the infill material, CDP has been used to model the compressive behaviour, whereas the tensile response has been described by a multi-linear stress-strain law (elastic, with hardening followed by perfect plasticity, Figure 8a), without defining a damage

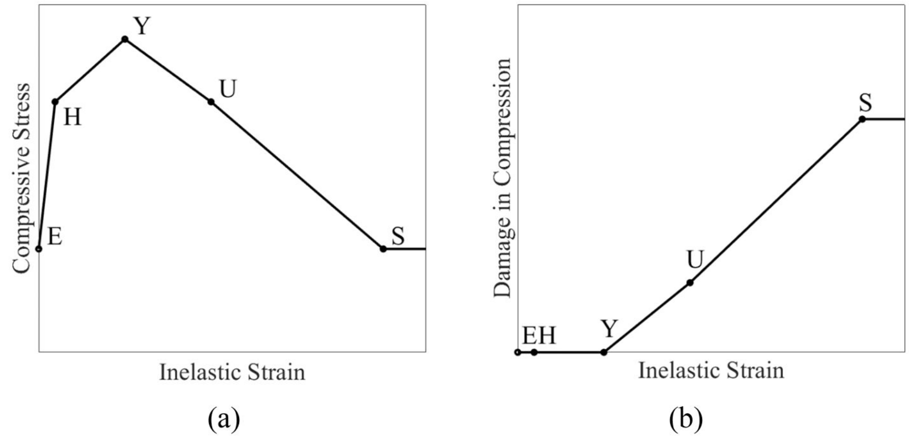

Figure 4. Schematisation of the compressive behaviour adopted for materials: (a) post-elastic skeleton curve; (b) inelastic strain – damage in compression curve.

Table 3. Definition of the characteristic points of the skeleton curve in compression.

Point	Inelastic strain $\tilde{\varepsilon}_c^{in}$ [-]	Uniaxial compressive stress σ_c [MPa]	Damage in compression d_c [-]
E	0.00	$0.33 \cdot \sigma_{c,y}$	0.00
H	$\frac{(0.80-0.33)\sigma_{c,y}}{E_1}$	$0.80 \cdot \sigma_{c,y}$	0.00
Y	$\frac{(1-0.80)\sigma_{c,y}}{0.1 \cdot E_0} + \varepsilon_H$	$\sigma_{c,y}$	0.00
U	$2 \cdot \varepsilon_H$	$0.80 \cdot \sigma_{c,y}$	$1 - \frac{\sigma_U}{\sigma_{c,y}}$
S	$4 \cdot \varepsilon_H$	$0.33 \cdot \sigma_{c,y}$	$1 - \frac{\sigma_S}{\sigma_{c,y}}$

variable. A CDP-like yield function, anyway, has been assigned to the infill.

In CDP, cracks' development is modelled through the assumption of a scalar isotropic damage with distinct damage parameters in tension and in compression. The yield function used is a modified Drucker-Prager one, controlled by the plastic strain variables evaluated at each integration point and characterised by non-associated plastic flow condition. The model requires the assignment of a set of parameters to define the yield surface, flow-rule and visco-plastic regularisation. For further details, the reader is addressed to the Abaqus manual (Dassault Systemes Simulia Corporation, 2011):

- ψ, dilatancy angle measured in the p-q plane, where p is the hydrostatic pressure and q the Von Mises equivalent stress.
- ϵ, eccentricity of the potential flow rule.
- ${}^{\sigma_{b0}}/_{\sigma_{c0}}$, ratio between the equi-biaxial compressive initial yielding stress and the uniaxial compressive initial yielding stress.
- $K_C = {}^{q_{TM}}/_{q_{CM}}$, parameter that modifies the Drucker-Prager yield function, being q_{TM} the second stress invariant on the tensile meridian and q_{CM} the second stress invariant on the compressive meridian.
- μ, viscosity parameter resulting from the use of a generalised Duvaut-Lions regularisation (Duvaut & Lions, 1972). It represents the relaxation time of the visco-plastic system and allows to improve the convergence rate. In this respect, it was observed in Rainone et al. (2023) that this parameter actually modifies the result of the analyses, however, it is essential to obtain convergence in these numerical applications in case of complex geometries and materials.

For all structural materials, given the absence of specific experimental data, the following values have been assumed: $\psi = 10°$; $\epsilon = 0.1$; ${}^{\sigma_{b0}}/_{\sigma_{c0}} = 1.16$; $K_C = 2/3$; $\mu = 0.01$. These values are in agreement with experimental evidence reported in the literature. The following sub-sections present the specific aspects of the uniaxial compressive and tensile post-elastic response adopted for the materials according to Abaqus formulation.

3.2.1. Definition of the uniaxial compressive response

For the compressive skeleton curve, in order to consider the effects of micro-cracks under small load increments and model damage development, a multi-linear stress-strain law characterised by hardening and subsequent softening is adopted, as schematically shown in Figure 4a. The material has an initial linear elastic response with undamaged stiffness E_0, until point E. Once a threshold of "micro-cracking" (point H) has been exceeded, the stiffness decays to half a value (cracked stiffness, E_1). After the stress peak $\sigma_{c,y}$, (point Y), the law is characterised by a marked softening, truncated at point S and indefinitely extended to ensure numerical stability. Regarding the damage model in compression, CDP assumes that failure is governed by a crushing mechanism by means of a hardening variable $\tilde{\varepsilon}_c^{pl}$, defined as "compressive equivalent plastic strain", that is related to the compressive inelastic strain $\tilde{\varepsilon}_c^{in}$, to the actual compressive stress state σ_c and to the compressive damage variable d_c:

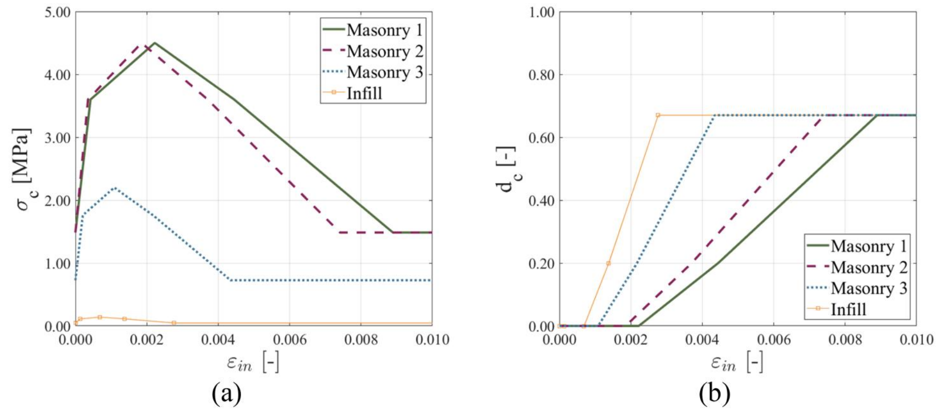

Figure 5. Compressive behaviour of the four materials: (a) post-elastic skeleton curves in compression; (b) inelastic strain - damage curves.

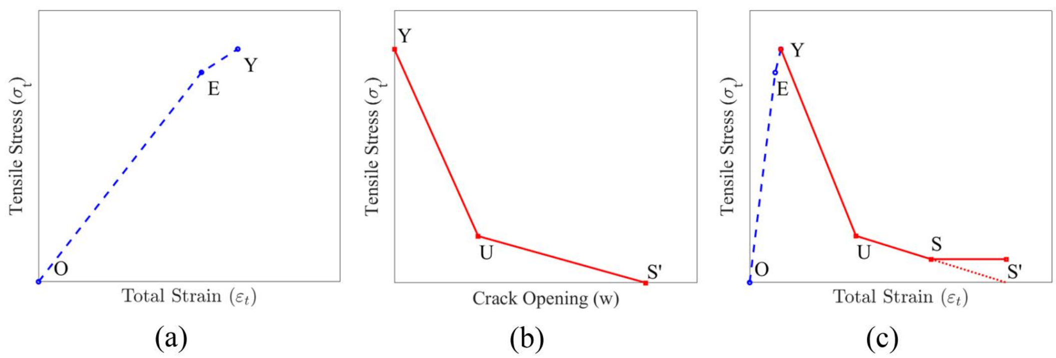

Figure 6. Modelling the tensile failure of masonry: (a) stress-strain relation for undamaged masonry; (b) stress-crack opening relation; (c) tensile law adopted.

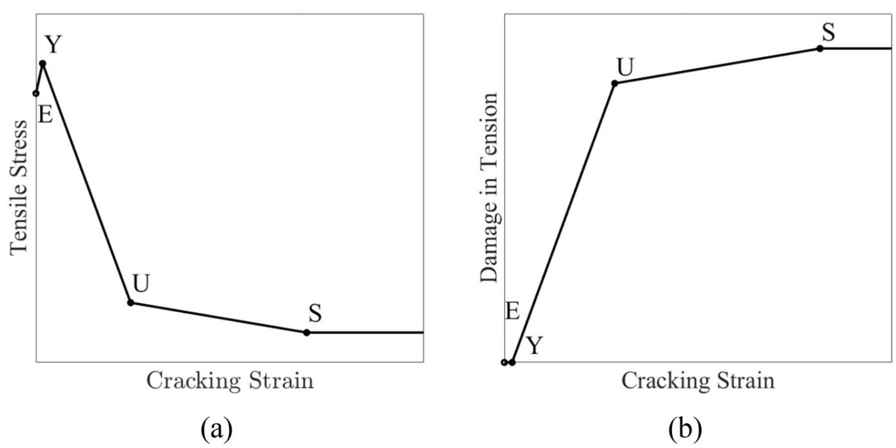

Figure 7. Schematisation of the tensile behaviour adopted: (a) inelastic strain - tensile yield stress curve; (b) inelastic strain - damageT curve.

Table 4. Characteristic points of the tensile skeleton curve ("m" is the average mesh size).

Point	Cracking strain ε_{ck} [-]	Uniaxial tensile stress σ_t [MPa]	Damage variable in tension d_t [-]
E	0.00	$0.90{\cdot}\sigma_{t,y}$	0.00
Y	$\frac{0.1\cdot\sigma_{t,y}}{E_1}$	$\sigma_{t,y}$	0.00
U	$\frac{G_t}{\sigma_{t,y}}\cdot\frac{1}{m}+\varepsilon_Y$	$0.20{\cdot}\sigma_{t,y}$	$1-\frac{\sigma_U}{\sigma_{t,y}}$
S	$\frac{2.5\cdot G_t}{\sigma_{t,y}}\cdot\frac{1}{m}+\varepsilon_Y$	$0.10{\cdot}\sigma_{t,y}$	$1-\frac{\sigma_S}{\sigma_{t,y}}$

$$\tilde{\varepsilon}_c^{pl} = \tilde{\varepsilon}_c^{in} - \frac{d_c}{(1-d_c)}\cdot\frac{\sigma_c}{E_0} \tag{1}$$

The damage variable governs the degradation of the elastic stiffness E_0 during the loading history: $E_{degraded} = (1-d_c)\cdot E_0$, and is assumed to be linearly dependant from the actual stress state σ_c according to Equation 2, in which $\sigma_{c,y}$ is the compressive strength of the material:

$$d_c = 1 - \frac{\sigma_c}{\sigma_{c,y}} \tag{2}$$

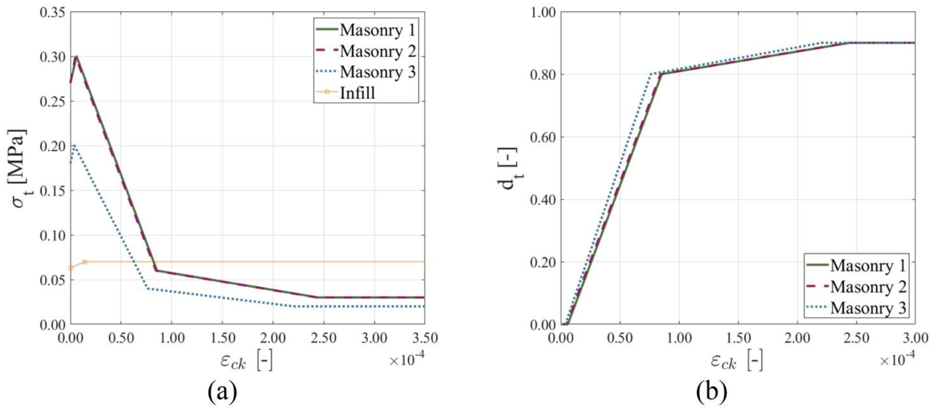

Figure 8. Tensile behaviour of the masonry materials: (a) inelastic strain - tensile yield stress curves; (b) inelastic strain - damage curves.

For each material, the characteristic points of the skeleton curve in compression are determined by specifying the above-mentioned parameters, as summarised in Table 3.

At each stress state, the value of the damage variable d_c is determined assuming that the damage in compression is triggered when the compressive peak stress value $\sigma_{c,y}$ is reached. The evolution of the damage variable is schematically represented in Figure 4b. It should be noted that the definition of d_c must comply with certain restrictions: in general, it must be satisfied that $d_c \leq 0.99$ ($d_c = 1.00$ would represent a total loss of stiffness, that can never be reached). Moreover, since the crushing process always involves energy dissipation, the compressive equivalent plastic strain cannot be negative and can never decrease with the increase of the inelastic strain. In order to satisfy this condition, it must be: $d_c \leq 0.67$. Figure 5a and Figure 5b show, respectively, the plots of the post-elastic skeleton curves and of the laws of the compressive damage against the inelastic strain for the four materials of the bridge.

3.2.2. Definition of the uniaxial tensile response

The tensile constitutive relation has been implemented with some adaptions with respect to the standard CDP Abaqus model. When dealing with the dynamics of masonry buildings, in fact, it is well known that the stiffness measured from ambient vibration tests, that engage very low energy levels, is significantly higher than the "secant" stiffness that corresponds to the natural vibration modes evaluated under moderate seismic actions. This is a consequence of the reduction of the effective elastic modulus due to micro-cracking, which is not activated at the very low stresses due to ambient vibrations. Based on these considerations, the skeleton curve has been modified with a bilinear branch until the peak, according to Figure 6a.

A second adaptation has been implemented in the post-peak behaviour. CDP provides a definition of the softening skeleton curve by means of a set of characteristic points that must be assigned by the user. The main problem is the choice of these parameters, for which no reliable experimental onsite test is actually available. Thues, it has been decided to adopt the provisions of Model Code (Fédération Internationale du Béton, 2010) regarding the tensile failure of concrete, expressed in terms of tensile strength - crack-opening width (w) relationship, as shown in Figure 6b. This law has been first converted into total strain components and then joined with the diagram of Figure 6a, obtaining the constitutive relationship of Figure 6c.

The material has an initial linear elastic response, with undamaged stiffness E_0, until the point E (representing a threshold of "micro-cracking"), after which the stiffness decays to half a value (cracked stiffness, E_1). After the tensile strength peak $\sigma_{t,y}$, (point Y), the curve is characterised by a bilinear softening branch (Y-U-S'), truncated at point S and indefinitely extended to ensure numerical convergence. The definition of the characteristic points of the skeleton curve requires to calculate the fracture energy G_t, which is made according to Equation 3 (Santinon et al., 2023):

$$G_t = 0.025 \left(\frac{\sigma_{c,y}}{10}\right)^{0.7} \tag{3}$$

The resulting values are: G_t= 14.295 N/m (for "*Masonry 1*" and "*Masonry 2*"); G_t= 8.662 N/m (for "*Masonry 3*"). The law implemented for the tensile behaviour is schematically shown in Figure 7a, whereas Table 4 reports the relationships that define the characteristic points.

Regarding the tensile damage model, CDP assumes that the failure is governed by a cracking mechanism related to a hardening variable $\tilde{\varepsilon}_t^{pl}$, defined as "tensile equivalent plastic strain". Similarly to the case of compression, the tensile equivalent plastic strain is related to the tensile cracking strain $\tilde{\varepsilon}_t^{ck}$ through Equation (4), as a function of the actual tensile stress state σ_t and of the tensile damage variable d_t:

$$\tilde{\varepsilon}_t^{pl} = \tilde{\varepsilon}_t^{ck} - \frac{d_t}{(1-d_t)} \cdot \frac{\sigma_t}{E_0} \tag{4}$$

The damage variable governs the degradation of the elastic stiffness E_0 according to the relation: $E_{degraded} = (1-d_t) \cdot E_0$ and is assumed to be linearly dependant from the actual stress state σ_t, according to Equation (5), in which $\sigma_{t,y}$ is the tensile strength of the material. For the tensile damage variable, it is assumed that $d_t \leq 0.90$:

$$d_t = 1 - \frac{\sigma_t}{\sigma_{t,y}} \tag{5}$$

For each stress state, the corresponding value of the damage variable is determined by assuming that the damage in

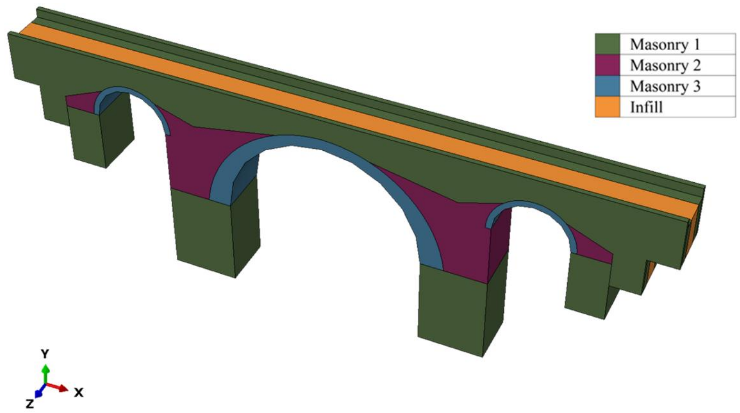

Figure 9. Solid Model – SM: geometry and materials assigned to the parts.

Figure 10. Mesh adopted for the Solid Model – SM.

tension starts when the tensile strength $\sigma_{t,y}$ is attained. The evolution of the damage variable is schematically represented in Figure 7b whereas the skeleton curves and damage evolution laws obtained for the four materials are plotted in Figure 8a and Figure 8b, respectively. It is worth remembering that, for the infill, the damage in tension was not defined.

3.3. Geometrical FE models

3.3.1. Numerical models implemented

For the case study of San Marcello Pistoiese bridge (Italy) (Leprotti et al., 2010; Pelà et al., 2009; 2013), two types of FE models have been developed in the Abaqus environment. The first one, which will be referred to as "Solid Model" (SM), is a complete three-dimensional, realistically detailed FE model, in which all structural elements are modelled with their actual geometry by solid elements. The second model, referred to as "Shell-Box Model" (SBM), is also a three-dimensional FE model but, in order to reduce the number of degrees of freedom of the problem, it features a simplified geometry reproduced by shell elements. The Solid Model is taken as a benchmark for calibrating the inertial and modal parameters of the Simplified Shell-Box Model. Then, the validation of the Simplified Model is performed through static non-linear analyses. The same analysis flow and the same boundary conditions are adopted for both models.

3.3.1.1. The complete Solid Model – SM. The SM is aimed at accurately representing the geometry of the structure by using three-dimensional solid Finite Elements (the z-axis is normal to the plane containing the three arches). The different materials of the bridge (with their constitutive laws, as defined in the previous section) have been assigned to each element according to the available information (Figure 9) and elements have been then assembled by simulating a full contact. A mesh consisting of elements of type C3D4 (tetrahedral element of first order, with constant stress) with an average size of 0.60 m was then implemented, for a total number of 169080 elements (Figure 10).

As mentioned in the introduction, the comparison with the available experimental data in terms of vibration frequencies and modal shapes has allowed the calibration of some parameters of the numerical Solid Model (in particular, those that were not provided by the experimental campaign or that were very scattered). According to the experimental dynamic identification (Leprotti et al., 2010; Pelà et al., 2009; 2013), the period of the 1st vibration mode is $T_1 = 0.250$ s, whereas the period of the 1st vibration mode for the numerical Solid Model "SM" has been found to be $T_1 = 0.266$s (Shapes are shown in Figure 15), showing a nearly perfect correspondence

3.3.1.2. The simplified Shell-Box Model - SBM. The SBM is again a three-dimensional model (Figure 11a), but the detail

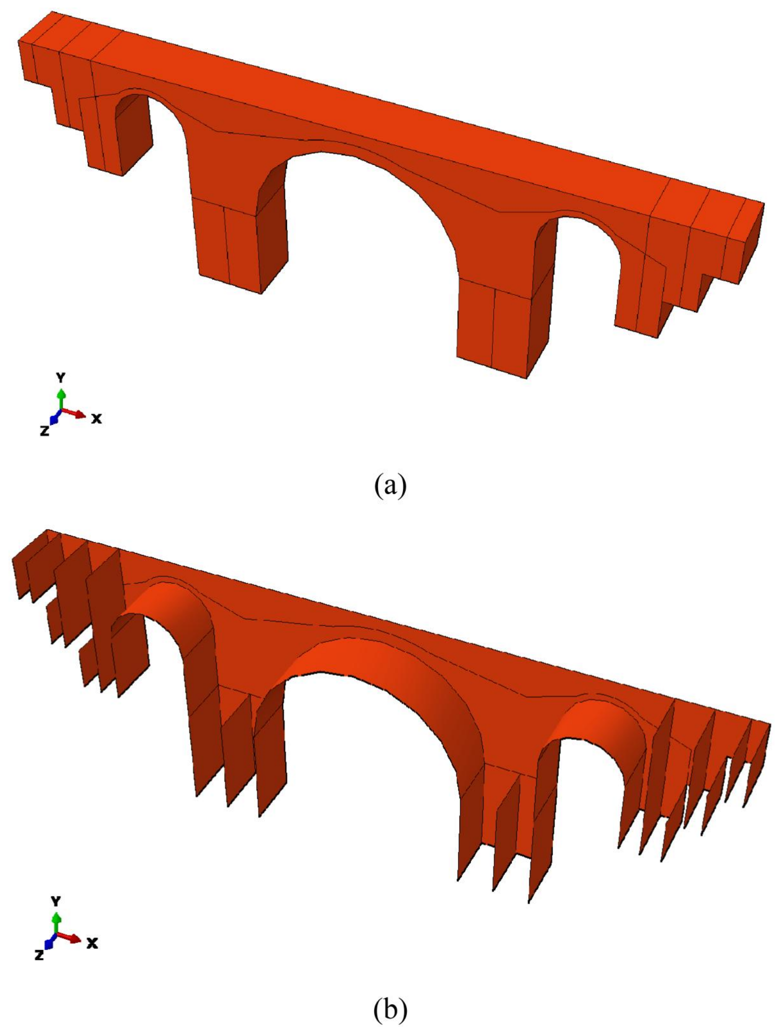

Figure 11. Geometry of the Shell-Box Model: (a) external; (b) internal.

of the structural geometry has been simplified by adopting shell elements in full contact (Figure 11b). Since an "equivalent" model is being defined, with a fictitious geometry that will be properly calibrated to match the modal response, and considering also that the differences among the parameters of Masonry 1, 2, 3 are minimal, only two materials have been considered: "*Masonry 1*", for all masonry parts, and "*Infill*" for the inner parts of backfill (Figure 13a). The thickness of the shells (Figure 13b) has been defined through the calibration process discussed in Section 3.3.2. The final FE mesh has an average size of 1.20 m, locally refined at the arches. Overall, it consists of 9080 S3-type elements (triangular shell elements with linear interpolation) (Figure 12) with a 95% reduction of the degrees of freedom with respect to the SM.

3.4. Calibration strategy and analysis workflow

The implementation and analysis of the two models is made following the steps shown in the flow-chart of Figure 14: (i) Collecting information about the case study; (ii) Solid-Model implementation; (iii) Shell-Box Model calibration; (iv) Shell-Box Model validation. The first step of the modelling and analysis process for an existing structure is the "Knowledge process", i.e., the retrieval of all existing documents and data; the execution of on-site inspections and tests for the characterisation of structural geometry and the assessment of mechanical properties of materials. In the developed procedure, a case study has been selected from the literature that refers to a real bridge for which surveys and direct investigation and tests were performed by others, so it was not directly experimentally investigated by us, but gave the opportunity of having a sufficient set of data. The case chosen represents quite well the typical real-practice situations. Regarding the Knowledge Process, the collected data have been derived by the previous experimental studies, among which there was a dynamic identification test to determine the frequency of the first vibration mode (this is typically out-of-plane, easier to determine in masonry arch bridges than higher modes).

Based on the knowledge achieved, the implementation of the detailed Solid Model involves the definition of the model geometry and constitutive laws of materials, the execution of linear analyses (to verify the correspondence of modal parameters with those obtained from the experimental dynamic identification provided by literature), the

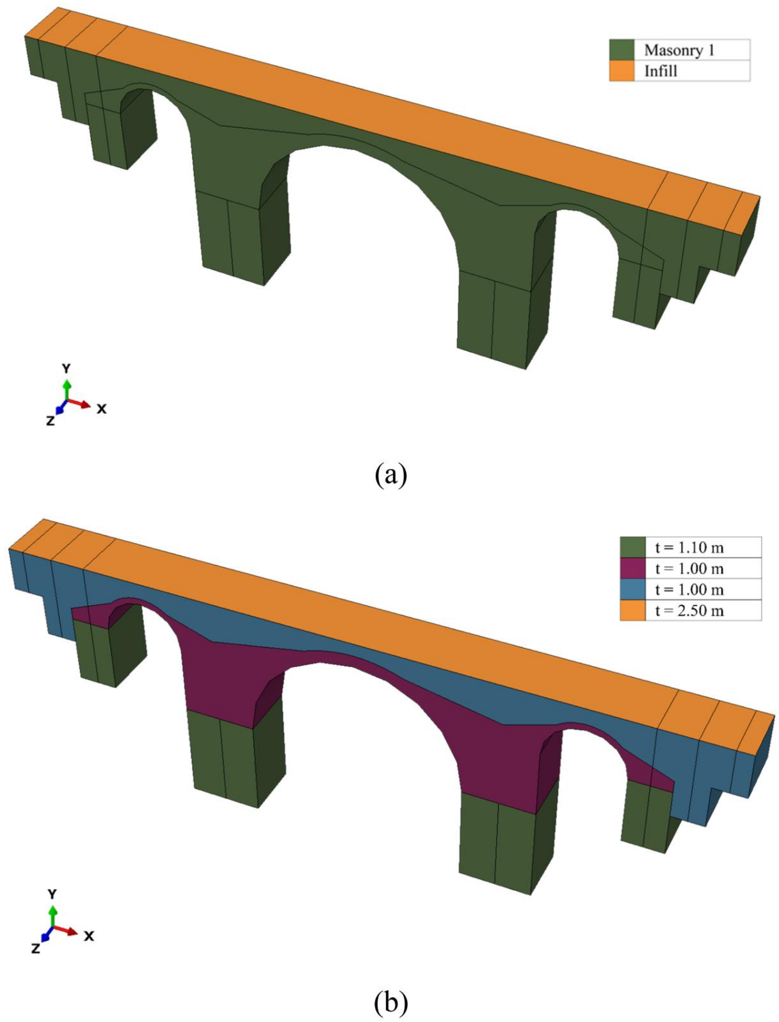

Figure 13. Materials (a) and sections (b) assigned to the different parts of the Shell-Box Model.

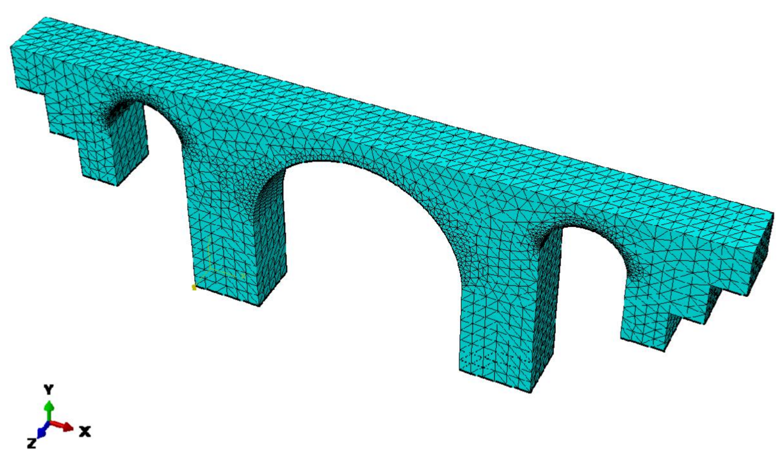

Figure 12. Mesh adopted for the Shell-Box Model.

execution of non-linear static analyses to provide the push-over curves useful for the subsequent steps of the procedure. The calibration process of the Shell-Box Model involves an iterative process in which the parameters that are varied are the thicknesses of the shell elements, by using a *trial-and-error* approach. The steps are the following (Figure 14): assignment of the thicknesses for all the shell elements composing the equivalent "box"; evaluation of the inertial characteristics and verification of their correspondence with the Solid Model; computation of the shape and frequencies of the vibration modes and verification of their correspondence with the Solid Model.

The next phase, called "validation", is aimed at guaranteeing the match of the two models in the non-linear field. The post-elastic parameters of the CDP model for the Shell-Box have been calibrated until obtaining a capacity curve

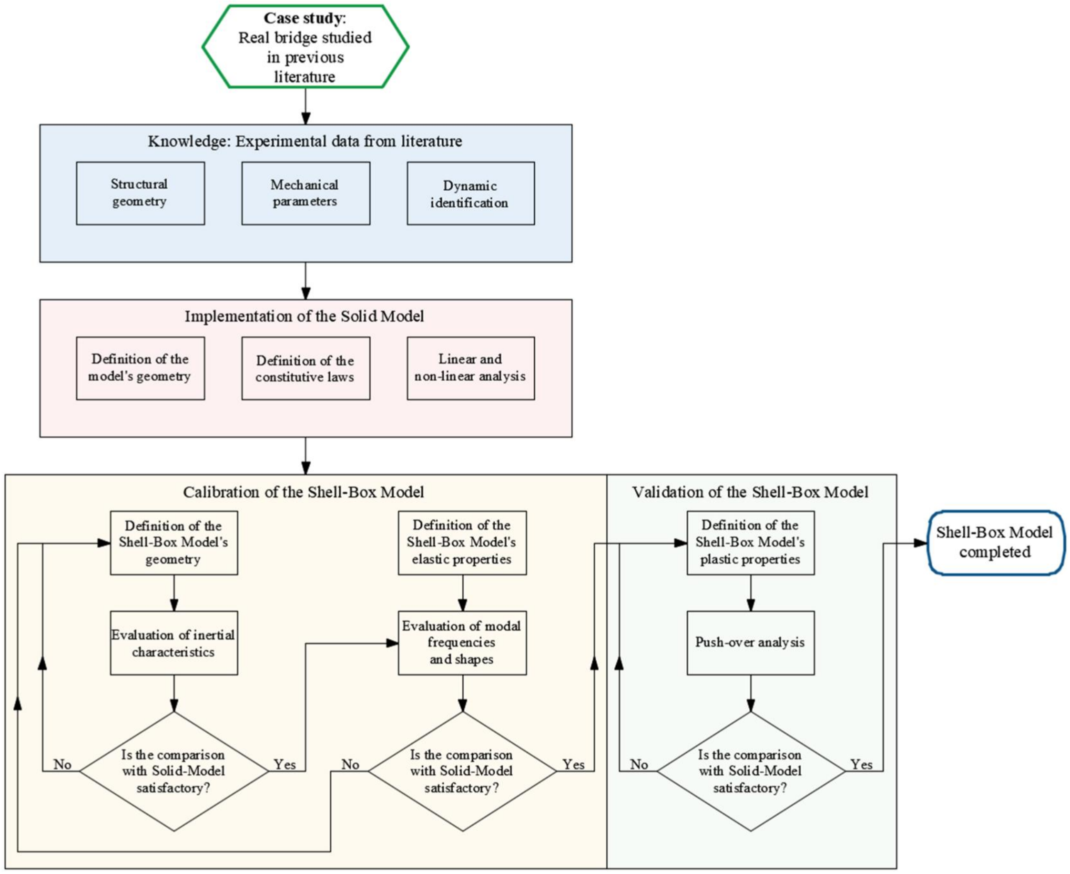

Figure 14. Analysis workflow: from calibration to validation.

Table 5. Inertial characteristics of models.

Entity	Solid model	Shell-Box model	Difference
Mass [kg]	$8402.88 \cdot 10^3$	$8001.33 \cdot 10^3$	−4.78 %
I_{XX}^{G} [kg·m^2]	$3.89 \cdot 10^8$	$4.15 \cdot 10^8$	6.68 %
I_{YY}^{G} [kg·m^2]	$3.42 \cdot 10^9$	$3.70 \cdot 10^9$	8.27 %
I_{ZZ}^{G} [kg·m^2]	$3.76 \cdot 10^9$	$4.04 \cdot 10^9$	7.31 %

Table 6. Comparison between Solid model and Shell-Box model in terms of the period of the first three vibration modes.

	Period T [s]		
Mode	Solid model	Shell-Box model	Difference
Mode I	0.266 s	0.267 s	0.25 %
Mode II	0.145 s	0.147 s	1.21 %
Mode III	0.093	0.104 s	11.51 %

Table 7. Comparison between Solid model and Shell-Box model in terms of the pseudo-spectral acceleration.

Mode #	Entity	Solid model	Shell-Box model	Difference
Mode I	$Se^{horizontal}$ [g]	0.554	0.554	0.00 %
	$Se^{vertical}$ [g]	0.207	0.206	−0.23 %
Mode II	$Se^{horizontal}$ [g]	0.554	0.554	0.00 %
	$Se^{vertical}$ [g]	0.359	0.359	0.00 %
Mode III	$Se^{horizontal}$ [g]	0.554	0.554	0.00 %
	$Se^{vertical}$ [g]	0.359	0.359	0.00 %

sufficiently comparable to that of the Solid Model. If so, the implementation process is complete, otherwise steps are repeated. The above-described workflow is graphically represented in Figure 14. It is worth noting that the definition of a cost-effective FE model for the real bridge case study through the process of implementation, calibration, validation has proven to be computationally feasible. Elastic analyses, even if extensive, are always inexpensive. The only time-consuming part is the non-linear analysis on the full model, which needs to be performed only once, while the non-linear analyses on the reduced model are undemanding and can be performed in large numbers. The goal, in fact, to include the procedure in a probabilistic analysis contest and handle uncertainties, for example through Monte-Carlo simulations.

4. Discussion of results

The results provided by the validation process have shown that the reduced SBM is able to catch the essential features of the full Model and can effectively replace it in linear and non-linear analyses. Its performance has been evaluated in terms of inertial characteristics, modal characteristics; design spectral acceleration, capacity curves and damage maps.

4.1. Inertial and modal characteristics

The inertial characteristics object of comparison include mass, centre of mass position and moments of inertia with respect to the principal barycentric axes. Regarding the position of the centre of mass along X and Z-directions, no significant differences between the two models have been found ($X_G^{SM} \approx X_G^{SBM}$; $Z_G^{SM} \approx Z_G^{SBM}$). Along the Y-direction, instead, a difference of 7.24% has been found ($Y_G^{SBM} - Y_G^{SM} = 1.12\ m$).

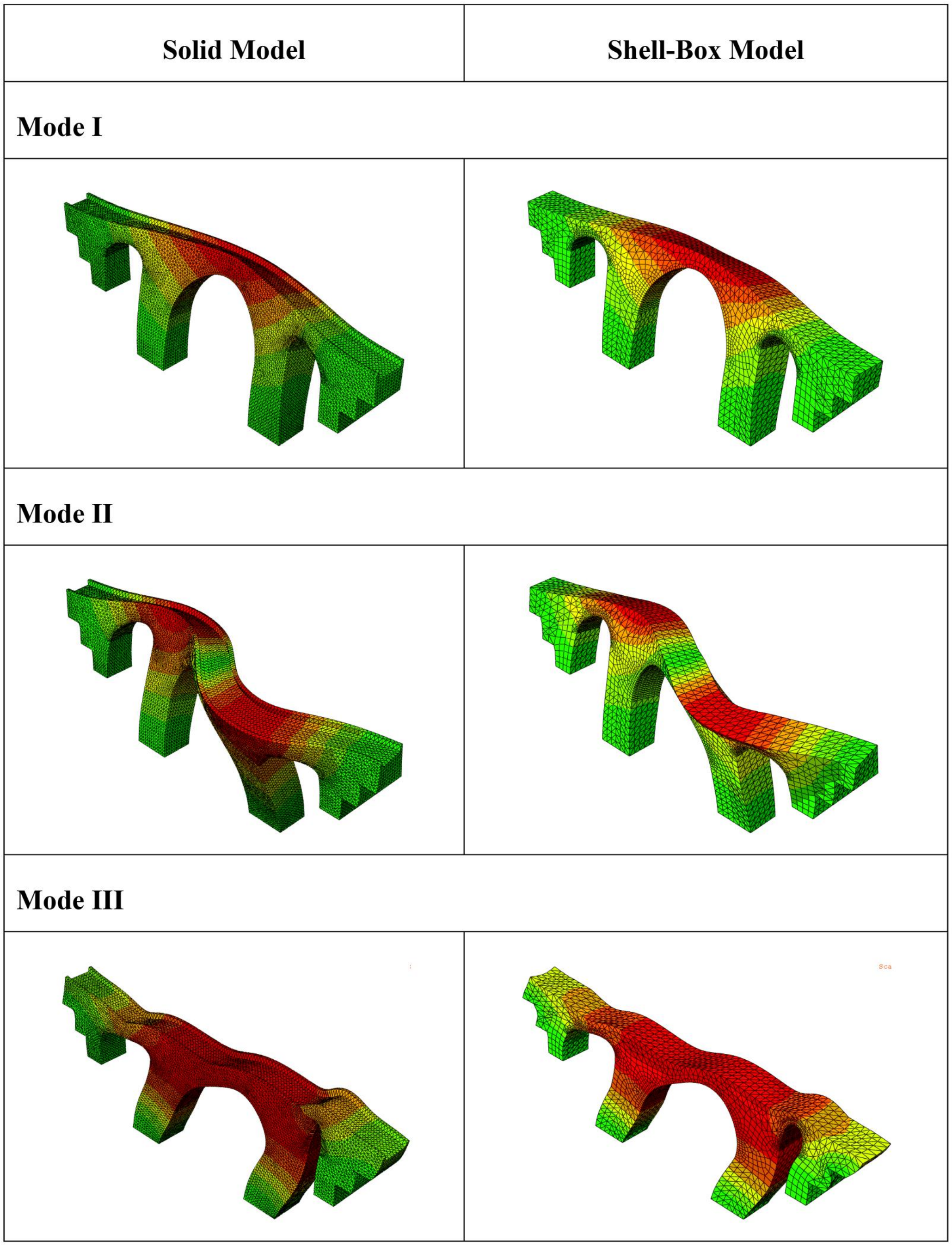

Figure 15. First three vibration modes of the two models: Solid Model (left); Shell-box Model (right).

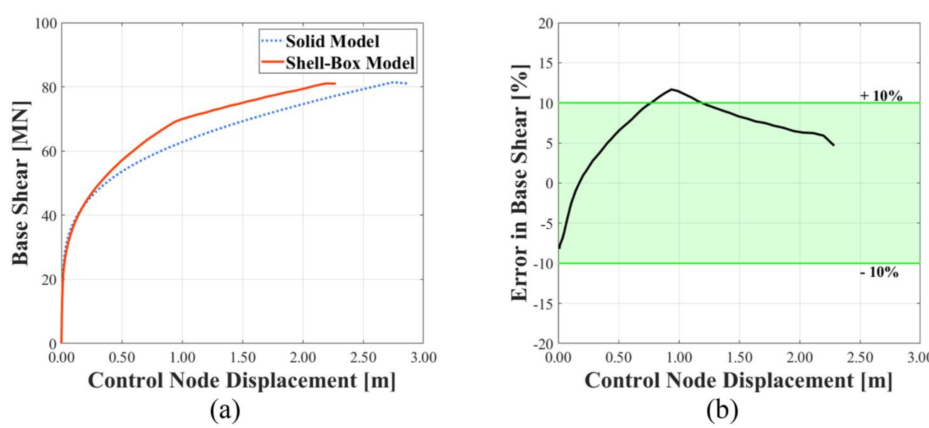

Figure 16. Comparison between Solid model and Shell-Box Model in the non-linear field. (a) Capacity curves of the two models until numerical collapse is attained; (b) plot of the differences in terms of base shear.

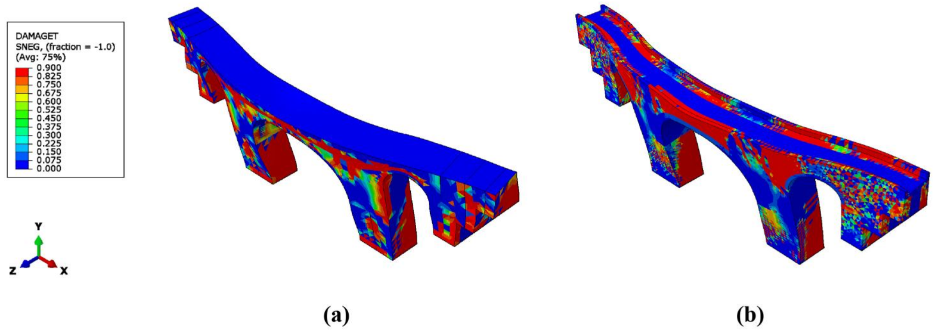

Figure 17. Map of damage variable in tension d_t in a 3D visualisation: (a) Shell-Box Model; (b) complete Solid Model.

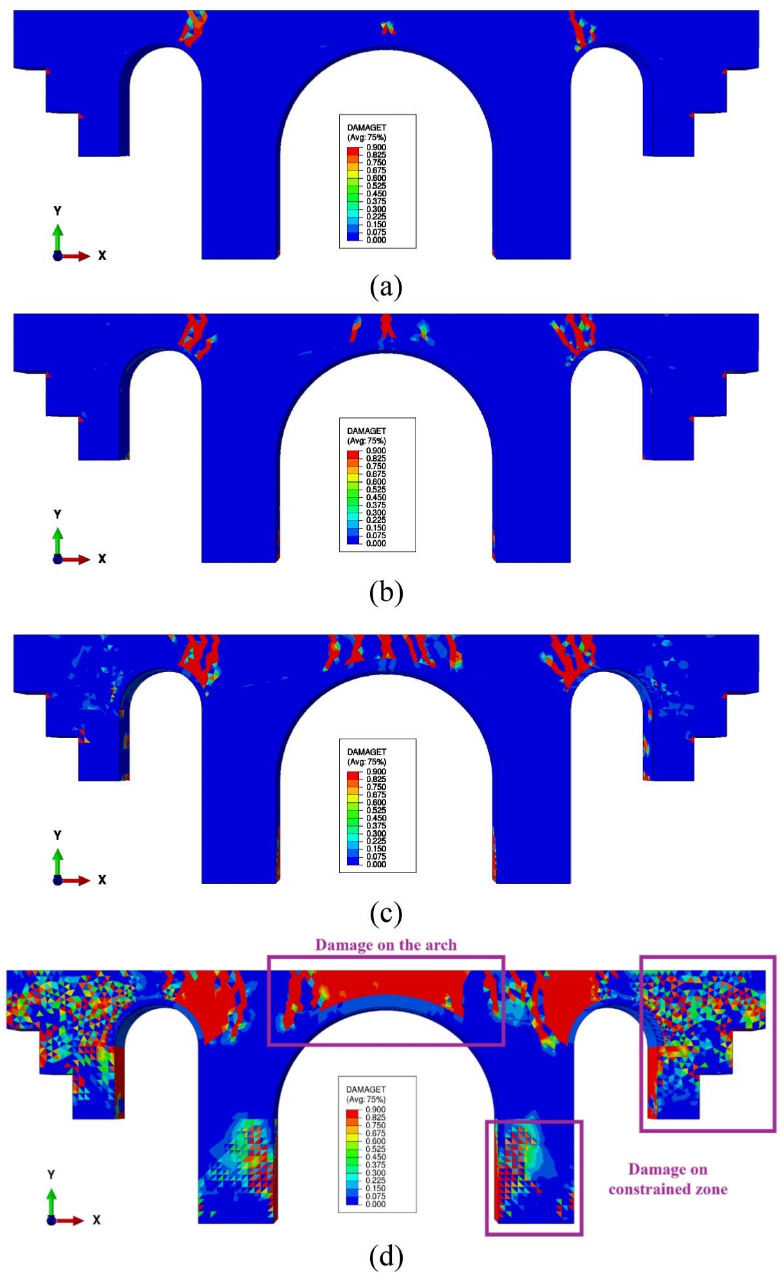

Figure 18. Damage of the Solid model on the façade + Z at drifts: (a) 0.40 cm; (b) 0.70 cm; (c) 1.00 cm; (d) 3.00 cm.

Table 5 shows the comparison between the inertial characteristics of the two models, where I_{XX}^G is the moment of inertia evaluated in the centre of mass with respect to the X-axis, I_{YY}^G with respect to the Y-axis and I_{ZZ}^G is the moment of inertia with respect to the Z-axis. For each of the parameter of interest, the last column of the table

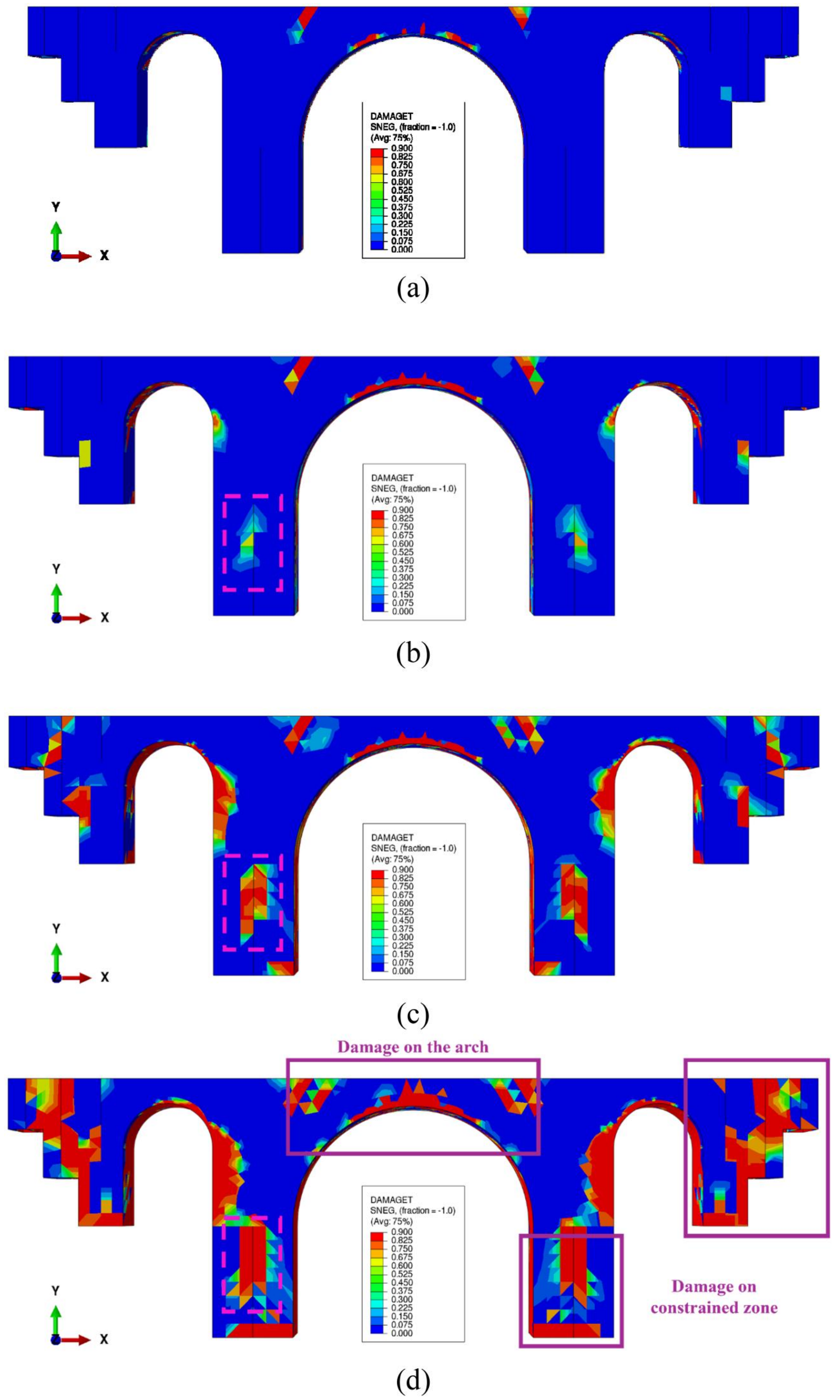

Figure 19. Damage of the Shell-Box Model on the façade + Z at drifts: (a) 0.40 cm; (b) 0.70 cm; (c) 1.00 cm; (d) 3.00 cm.

reports the difference found between the two models. A deviation in the +/- 10% range has been considered in line with the epistemic uncertainty in the knowledge of the structure. By this criterion, the approximation achieved by the SBM for the inertial characteristics can be considered good. For the modal parameters, the comparison has been performed with regard to the first three vibration modes (Table 6).

The 1st mode, or fundamental mode, is usually the most interesting one, since the largest displacements caused by seismic actions are mainly out of plane and therefore consistent with the 1st modal shape and for it, the difference observed in terms of frequency and period is within the +/- 10% range. Moving to the next modes, instead, the difference on period grows and for the third vibration mode goes beyond this range. However, this does not significantly affect the determination of the spectral pseudo-acceleration, which, in fact, exhibits a null variation on the horizontal and vertical components for all three modes (Table 7). The modal shape of the first three modes is the same for both models (Figure 15), and this confirms that the reduced SBM

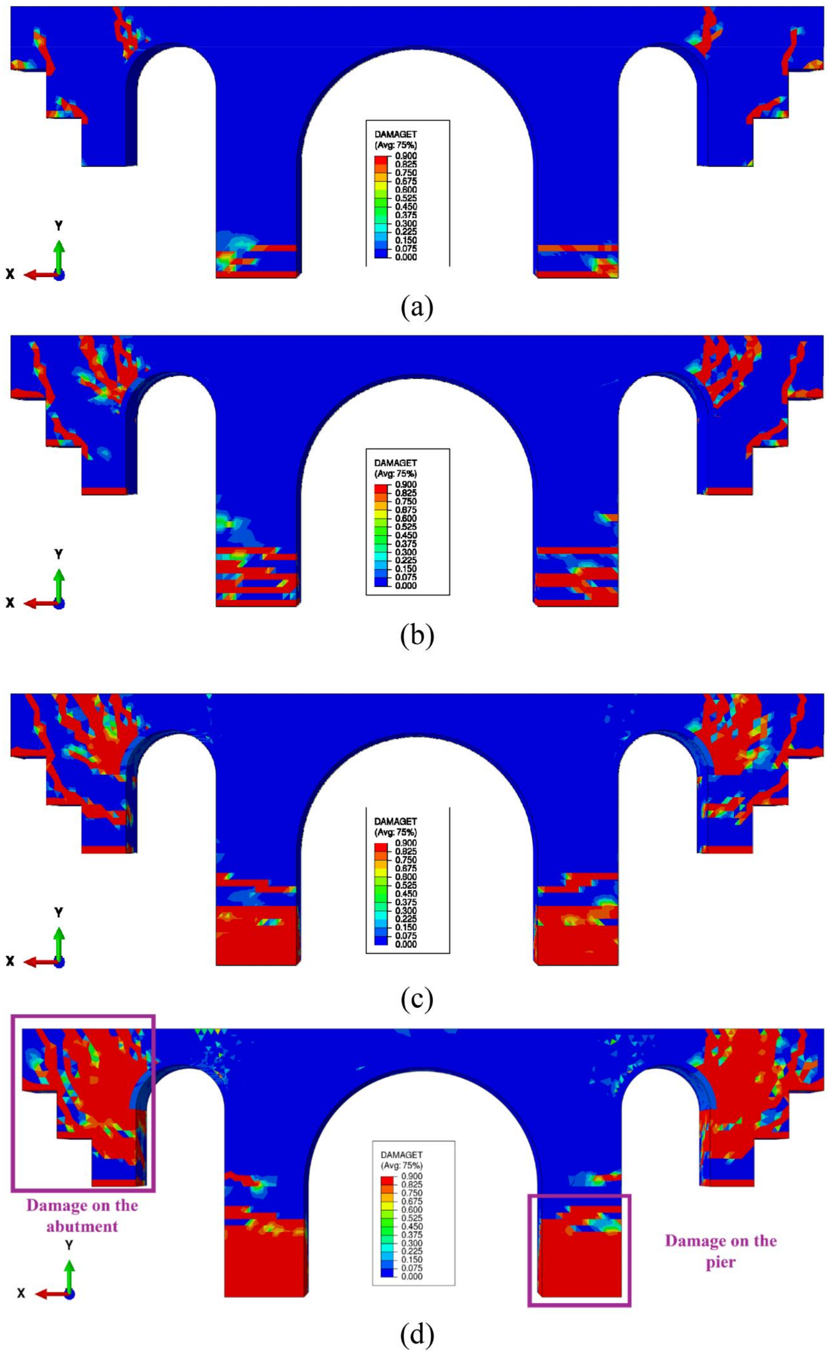

Figure 20. Damage of the Solid model on the façade -Z at drifts: (a) 0.40 cm; (b) 0.70 cm; (c) 1.00 cm; (d) 3.00 cm.

effectively retains the information about the dynamic behaviour of the structure and is an efficient option for performing both dynamic identification procedures and cost-effective non-linear dynamic analyses.

4.2. Post-elastic response: capacity curve and damage maps

Regarding the post-elastic behaviour of the structure, a pushover analysis has been performed on both models according to the directions +/- Z, assuming a load profile proportional to the mass distribution, and as a control point the central point CP of the upper plane (Figure 2, top). Since both models are symmetric with respect to the XY plane, the results are presented and discussed only for the + Z direction. From Figure 16a, which shows the capacity curves obtained for the complete and the reduced model, it can be noticed that the two models have given substantially identical results, both with regard to the initial elastic stiffness (as it was in fact to be expected, considering the good coincidence of the first vibration mode) and the post-elastic response (also reaching a peak force very similar).

For each value of the top control node displacement, the difference between the base shear values, evaluated on the reduced "SB" Model and on the complete model, has been calculated according to Equation (6) and plotted in Figure 16b. It can be noted that the difference is almost always

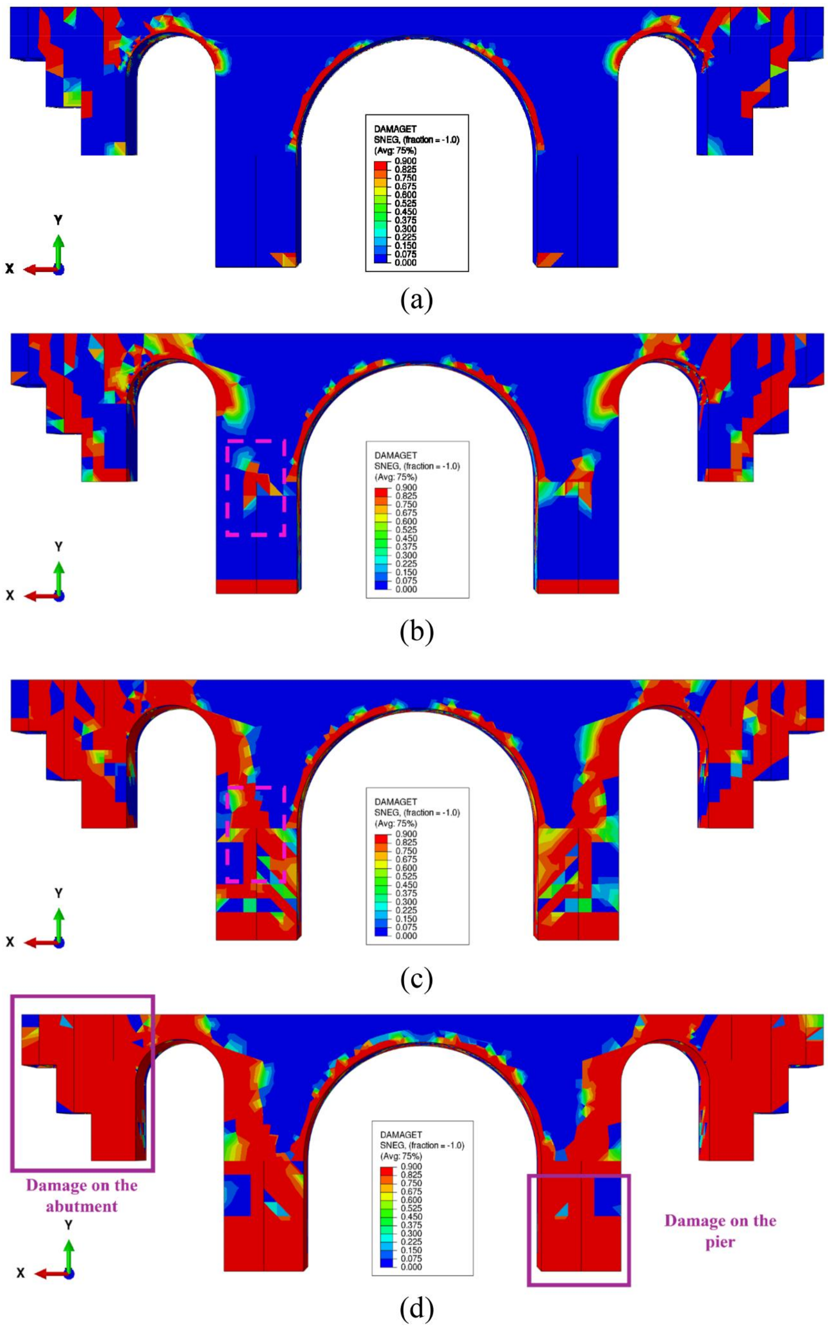

Figure 21. Damage of the Shell-Box Model on the façade -Z at drifts: (a) 0.40 cm; (b) 0.70 cm; (c) 1.00 cm; (d) 3.00 cm.

included within the range of +/- 10%, whereas the main difference is that the Solid Model takes about 70 h to run, while the Shell-Box model takes about 8 min, thus allowing a reduction in computation time of about 99.81%:

$$Error = \frac{V_{SB} - V_S}{V_S} \tag{6}$$

In the Solid Model, during the pushover analyses, the development of two main types of damage has been encountered. The first one occurs in the upper part of the arches, around the keystone (Figure 17(b); Figure 18) and affects the façade on outer side (with respect to the push-over direction, +Z). The second type of damage affects the pier bases, at the inner side of the bridge (-Z façade, Figure 17(b); Figure 20).

Overall, the Shell-Box Model is able to capture the general distribution of damage and the type of mechanism fairly well (Figure 17(a)). It should be noted that there are some localised areas where the damage map is slightly affected by the particular “Shell-Box” configuration of the reduced model, at the intersections between shells (outlined in Figure 19 and 21 in the magenta boxes). However, this is not indicative of a real localised damage, but strictly depends by the use of shell elements, that, although convenient from a computational point of view, lead to over-estimate damage in the areas of concentration of inelastic deformations. In a future systematisation of the interface of the procedure, the representation method could be calibrated with a post-processing capable of properly representing an "equivalent" smeared damage.

The reduced model, anyway, captures fairly well the qualitative distribution of damage on the keys of the arches of the + Z façade and in the area close to the constrained zones of the + Z and -Z façades, as shown in 3D in Figure 17, and, in plan view, in Figures 18, 19, 20, 21, in which this correspondence is indicated by the red boxes. The magenta-dotted boxes indicate the areas where spurious damage has developed in the shell model. Although the damage map is not as detailed and accurate as that of the solid model, it allows to interpret the collapse mechanism in a qualitatively correct way.

5. Conclusions

The procedure presented in the article proposes an approach for dealing with seismic vulnerability analyses of masonry bridges by calibrating an appropriate "reduced" FE model (Shell-Box Model, "SBM") that balance the degree of detail of spatial geometry and content in terms of constitutive modelling in view of an effective description of non-linear structural response in the dynamic range. The aim is to allow advanced structural analyses in the non-linear field while reducing the computational effort and opening the way to a cost-effective management of the many uncertainties that characterise the problem both in terms of knowledge of existing structures and of non-linear parameters of masonry materials, since it will be feasible to perform extensive parametric analyses in the non-linear dynamic field.

The reduced Shell-Box Model was calibrated against a reference, complete model ("Solid Model", SM), that was developed by referring to geometrical data and mechanical parameters provided by previous experimental tests and validated thanks to data from experimental dynamic identification. The reduced model provided values of the inertial characteristics that differ from the reference ones by less than 10%. The first natural mode of vibration is well approximated in terms of shape and period, allowing to use this simplified model in dynamic identification procedures. Despite the differences found in the periods of the second and third vibration mode are larger, the simplified model still allows to satisfactorily define the pseudo-spectral acceleration of the Italian Building Code, with results that are comparable to that the SM (Solid Model). Push-over analyses were carried out on the two models for reproducing the collapse mechanisms affecting the bridge subject to an out-of-plane seismic loading, and the results in terms of the capacity curve and damage maps were in a fair good agreement.

It is worth noting that the layout and characteristics of this reduced model have been specifically designed to capture the essential elements of structural response to seismic actions. It retains the fundamental elements of the overall geometry and nature of the materials, so as to allow a straightforward reading and interpretation of data on a global structural scale (e.g., displacements, deformations, and actions), but is not realistic in its details, and could not be suitable for representing load conditions different from those for which it was optimised. In the future it could be interesting, for example, to use the strategy for the analysis of the bridge under traffic loads, but the reduced model to develop should be differently designed and optimised. In the future development of the research work, these load situations will be investigated and developed, by selecting a more appropriate case study, which envisage relevant information about the experimental response under vertical loads (as, for instance, the experimental laboratory case study presented in Sarhosis et al., 2024).

The proposed modelling strategy offers a valuable tool for the structural assessment and seismic safety evaluation of masonry arch bridges, particularly in contexts where detailed information is limited and it is necessary to deal with the uncertainty related to geometry, material properties and seismic action. By enabling extensive non-linear analyses with significantly reduced computational effort, the proposed approach allows to implement a probabilistic approach, easily performing a large number of parametric non-linear dynamic analyses, supporting informed decision-making in the management, conservation, and retrofitting of existing bridges. Its applicability to real case studies, as demonstrated in this work, provides a practical framework for incorporating uncertainty and structural degradation into vulnerability assessments - key challenges in the preservation of historical masonry bridges.

Author contributions

CRediT: **Giuseppina Uva**: Conceptualization, Funding acquisition, Methodology, Supervision, Validation, Writing – original draft, Writing – review & editing; **Luigi S. Rainone**: Data curation, Formal analysis, Investigation, Software, Visualization, Writing – original draft; **Luis C. M. da Silva**: Data curation, Investigation, Software, Validation; **Siro Casolo**: Conceptualization, Methodology, Supervision, Validation, Writing – original draft, Writing – review & editing.

Disclosure statement

No potential conflict of interest was reported by the author(s).

Funding

This study was supported by FABRE - "Research consortium for the evaluation and monitoring of bridges, viaducts and other structures" (www.consorziofabre.it/en). Any opinion expressed in the paper does not necessarily reflect the view of the funder.

References

Addessi, D., Gatta, C., Nocera, M., & Liberatore, D. (2021). Nonlinear dynamic analysis of a masonry arch bridge accounting for damage evolution. *Geosciences*, *11*(8), 343. https://doi.org/10.3390/geosciences11080343

Addessi, D., Liberatore, D., & Nocera, M. (2022). Damaging behavior of masonry arch bridges: Analysis of 'Ponte delle Torri' in Spoleto, Italy. *Journal of Earthquake Engineering*, *26*(1), 449–474. https://doi.org/10.1080/13632469.2019.1690599

Bayraktar, A., & Hökelekli, E. (2021). Nonlinear soil deformability effects on the seismic damage mechanisms of brick and stone masonry arch bridges. *International Journal of Damage Mechanics*, *30*(3), 431–452. https://doi.org/10.1177/1056789520974423

Caliò, I., Marletta, M., & Pantò, B. (2012). A new discrete element model for the evaluation of the seismic behaviour of unreinforced masonry buildings. *Engineering Structures*, *40*, 327–338. https://doi.org/10.1016/j.engstruct.2012.02.039

Casolo, S., & Peña, F. (2007). Rigid element model for in-plane dynamics of masonry walls considering hysteretic behaviour and damage. *Earthquake Engineering & Structural Dynamics*, *36*(8), 1029–1048. https://doi.org/10.1002/eqe.670

Casolo, S., & Sanjust, C. A. (2009). Seismic analysis and strengthening design of a masonry monument by a rigid body spring model: The "Maniace Castle" of Syracuse. *Engineering Structures*, *31*(7), 1447–1459. https://doi.org/10.1016/j.engstruct.2009.02.030

Casolo, S., Diana, V., & Uva, G. (2017). Influence of soil deformability on the seismic response of a masonry tower. *Bulletin of Earthquake Engineering*, *15*(5), 1991–2014. https://doi.org/10.1007/s10518-016-0061-y

Crisafulli, F. J., Carr, A. J., & Park, R. (2005). Experimental response of framed masonry structures designed with new reinforcing details. *Bulletin of the New Zealand Society for Earthquake Engineering*, *38*(1), 19–32. https://doi.org/10.5459/bnzsee.38.1.19-32

D'Altri, A. M., Sarhosis, V., Milani, G., Rots, J., Cattari, S., Lagomarsino, S., Sacco, E., Tralli, A., Castellazzi, G., & De Miranda, S. (2020). Modeling strategies for the computational analysis of unreinforced masonry structures: Review and classification. *Archives of Computational Methods in Engineering*, *27*(4), 1153–1185. https://doi.org/10.1007/s11831-019-09351-x

Dassault Systemes Simulia Corporation. (2011). *Abaqus* (Version *6.11*) [Computer software]. https://www.3ds.com/products/simulia/abaqus

Drygala, I., Dulinska, J., Bednarz, Ł., & Jasienko, J. (2018). Numerical evaluation of seismic-induced damages in masonry elements of historical arch viaduct. *IOP Conference Series: Materials Science and Engineering*, *364*(1), 012006. https://doi.org/10.1088/1757-899X/364/1/012006

Duvaut, G., & Lions, J. L. (1972). *Les Inequations en Mecanique et en Physique*. Dunod.

Fédération Internationale du Béton. (2010). *Model Code 2010. Bulletin/Fédération Internationale du Béton*. International Federation for Structural Concrete (fib).

Forgács, T., Sarhosis, V., & Ádány, S. (2018). Discrete element modelling of skew masonry arch bridges taking into account arch ring-backfill interaction. *Proceedings of 10th IMC-International Masonry Conference*. Newcastle University.

Giaretton, M., Dizhur, D., da Porto, F., & Ingham, J. M. (2016). Construction details and observed earthquake performance of unreinforced clay brick masonry cavity-walls. *Structures*, *6*, 159–169. https://doi.org/10.1016/j.istruc.2016.04.004

Gönen, S., & Soyöz, S. (2021). Seismic analysis of a masonry arch bridge using multiple methodologies. *Engineering Structures*, *226*, 111354. https://doi.org/10.1016/j.engstruct.2020.111354

Lee, J., & Fenves, G. L. (1998). Plastic-damage model for cyclic loading of concrete structures. *Journal of Engineering Mechanics*, *124*(8), 892–900.) https://doi.org/10.1061/(ASCE)0733-9399(1998)124:8(892

Leprotti, L., Pelà, L., Aprile, A., & Benedetti, A. (2010). *Control node identification in nonlinear seismic analysis of masonry arch bridges* [Paper presentation]. Proceedings of the Eighth International Masonry Conference (pp. 1113–1122).

Liu, B., Drougkas, A., Sarhosis, V., Smith, C. C., & Gilbert, M. (2023). Experimental investigation on the shear behaviour of the brickwork-backfill interface in masonry arch bridges. *Engineering Structures*, *292*, 116531. https://doi.org/10.1016/j.engstruct.2023.116531

Lubliner, J., Oliver, J., Oller, S., & Oñate, E. (1989). A plastic-damage model for concrete. *International Journal of Solids and Structures*, *25*(3), 299–326. https://doi.org/10.1016/0020-7683(89)90050-4

Ministero delle Infrastrutture e dei Trasporti. (2018). Aggiornamento Delle «Norme Tecniche per le Costruzioni», Decreto Ministeriale 17 Gennaio 2018, Supplemento Ordinario Alla "Gazzetta Ufficiale" n. 42 Del 20 Febbraio 2018 - Serie Generale.

Ministero delle Infrastrutture e dei Trasporti. (2019). Istruzioni per L'applicazione Dell'«Aggiornamento Delle "Norme Tecniche per le Costruzioni"» di Cui al Decreto Ministeriale 17 Gennaio 2018, Supplemento Ordinario Alla "Gazzetta Ufficiale" n. 35 Del 11 Febbraio 2019 - Serie Generale.

Modena, C., Tecchio, G., Pellegrino, C., da Porto, F., Donà, M., Zampieri, P., & Zanini, M. A. (2015). Reinforced concrete and masonry arch bridges in seismic areas: Typical deficiencies and retrofitting strategies. *Structure and Infrastructure Engineering*, *11*(4), 415–442. https://doi.org/10.1080/15732479.2014.951859

Oliveira, D. V., Lourenço, P. B., & Lemos, C. (2010). Geometric issues and ultimate load capacity of masonry arch bridges from the northwest Iberian Peninsula. *Engineering Structures*, *32*(12), 3955–3965. https://doi.org/10.1016/j.engstruct.2010.09.006

Pelà, L., Aprile, A., & Benedetti, A. (2009). Seismic assessment of masonry arch bridges. *Engineering Structures*, *31*(8), 1777–1788. https://doi.org/10.1016/j.engstruct.2009.02.012

Pelà, L., Aprile, A., & Benedetti, A. (2013). Comparison of seismic assessment procedures for masonry arch bridges. *Construction and Building Materials*, *38*, 381–394. https://doi.org/10.1016/j.conbuildmat.2012.08.046

Rainone, L. S., Tateo, V., Casolo, S., & Uva, G. (2023). About the use of concrete damage plasticity for modeling masonry post-elastic behavior. *Buildings*, *13*(8), 1915. https://doi.org/10.3390/buildings13081915

Rinaldin, G., Amadio, C., & Macorini, L. (2016). A macro-model with nonlinear springs for seismic analysis of URM buildings. *Earthquake Engineering & Structural Dynamics*, *45*(14), 2261–2281. https://doi.org/10.1002/eqe.2759

Santinon, D., Zampieri, P., Pellegrino, C., Ricci, D., Iodice, F., Vecchi, A., & Iacobini, F. (2023). Numerical approaches to assess the load capacity of FRCM strengthened masonry bridges. In F. Biondini & D. M. Frangopol (Eds.), *Life-cycle of structures and infrastructure systems* (pp. 1560–1566). CRC Press.

Sarhosis, V., Liu, B., & Gilbert, M. (2024). The 3d response of a large-scale masonry arch bridge - part I: Performance under low and medium loading levels. *Engineering Structures*, *316*, 118496. https://doi.org/10.1016/j.engstruct.2024.118496

Smith, C., Gilbert, M., & Callaway, P. (2004). *Geotechnical issues in the analysis of masonry arch bridges* [Paper presentation]. Proceedings of the 4th international arch bridges conference (pp. 343–352).

Tecchio, G., Donà, M., Saler, E., & da Porto, F. (2023). Fragility of single-span masonry arch bridges accounting for deterioration and damage effects. *European Journal of Environmental and Civil Engineering*, *27*(5), 2048–2069. https://doi.org/10.1080/19648189.2022.2108504

Tubaldi, E., Macorini, L., & Izzuddin, B. A. (2020). Identification of critical mechanical parameters for advanced analysis of masonry arch bridges. *Structure and Infrastructure Engineering*, *16*(2), 328–345. https://doi.org/10.1080/15732479.2019.1655071

Zani, G., Martinelli, P., Galli, A., & di Prisco, M. (2020). Three-dimensional modelling of a multi-span masonry arch bridge: Influence of soil compressibility on the structural response under vertical static loads. *Engineering Structures*, *221*, 110998. https://doi.org/10.1016/j.engstruct.2020.110998

Zizi, M., Chisari, C., & De Matteis, G. (2023). Effect of the backfill material in the seismic response of multi-span masonry arch bridges under seismic loading. *Procedia Structural Integrity*, *44*, 673–680. https://doi.org/10.1016/j.prostr.2023.01.088